SCIENTIFIC REPORTS

OPEN

SUBJECT AREAS:
MECHANICAL AND STRUCTURAL PROPERTIES AND DEVICES
NEMS

Received
6 March 2014

Accepted
15 April 2014

Published
2 May 2014

Correspondence and requests for materials should be addressed to F.G. (francois.grey@cern.ch) or Q.Z. (zhengqs@tsinghua.edu.cn)

The high-speed sliding friction of graphene and novel routes to persistent superlubricity

Yilun Liu[1,2], François Grey[2,3,4,5] & Quanshui Zheng[2,6]

[1]International Center for Applied Mechanics, SV Lab, School of Aerospace, Xi'an Jiaotong University, Xi'an 710049, China, [2]Centre for Nano and Micro Mechanics, Tsinghua University, Beijing 100084, China, [3]Department of Physics, Tsinghua University, Beijing 100084, China, [4]London Centre for Nanotechnology, University College London, London WC1H OAH, U.K, [5]Centre Universitaire d'Informatique, University of Geneva, CH-1227 Carouge, Switzerland, [6]Department of Engineering Mechanics, Applied Mechanics Lab, and State Key Laboratory of Tribology, Tsinghua University, Beijing 100084, China.

Recent experiments on microscopic graphite mesas demonstrate reproducible high-speed microscale superlubricity, even under ambient conditions. Here, we explore the same phenomenon on the nanoscale, by studying a graphene flake sliding on a graphite substrate, using molecular dynamics. We show that superlubricity is punctuated by high-friction transients as the flake rotates through successive crystallographic alignments with the substrate. Further, we introduce two novel routes to suppress frictional scattering and achieve persistent superlubricity. We use graphitic nanoribbons to eliminate frictional scattering by constraining the flake rotation, an approach we call *frictional waveguides*. We can also effectively suppress frictional scattering by biaxial stretching of the graphitic substrate. These new routes to persistent superlubricity at the nanoscale may guide the design of ultra-low dissipation nanomechanical devices.

The nonlinear nature of friction at the nanoscale has sparked intense experimental and theoretical interest[1–3]. A focus of much of this research is on achieving superlubricity[4–6], a term originally introduced to describe ultra-low friction between rotationally misaligned – and hence incommensurate – crystalline lattices[7–9]. Superlubricity has been observed by Friction Force Microscopy, which typically operates at $\ll 1$ mm/s. However, for freely-moving nanoparticles at low velocities, superlubricity is suppressed because of spontaneous rotation into energetically favourable commensurate states, or "lock-in"[10,11], while the commensurate states are always the stable orbits for the sliding of the graphene flake[12,13]. Recent experimental results, however, show reproducible high-speed superlubricity in microscale graphite mesas (10×10 μm^2) under ambient conditions, where the highest speed is 25 m/s[14]. Besides, no lock-in is observed for a wide-range of rotational misalignments, due to much larger rotational inertia on the microscale[15]. In this study, we wish to explore in detail how the lock-in phenomenon disrupts superlubricity on the nanoscale, and consequently how we may design systems that suppress this effect, so that persistent superlubricity can be exploited for building efficient nanomechanical devices.

In recent simulations by Guerra et al.[16], a regime of "ballistic nanofriction" was observed for nanoclusters of gold moving at high velocity on graphite. A profound insight of this study is that in contrast to the much-studied low-velocity regime, at high velocities superlubricity is the norm, punctuated by transitory periods of lock-in where friction is high. Lebdeva et al.[17] have observed similar behavior in simulations of the thermally induced motion of nanoscale graphene islands on graphite.

Results

Here we introduce a simple mechanism to induce ballistic nanofriction in graphene nanoparticles, based on high-speed motion observed experimentally by shearing microscopic mesas of graphite, which occurs in order to minimize the free surface energy at the sheared interface[14,15,18]. From classical mechanics, it is straightforward to deduce an expression for the peak speed produced by this effect for shearing of a square flake of graphite from a fixed mesa: $v_{\max} = [(2/N)(s/l)(E_f/m_C)]^{1/2}$, where N is the number of graphitic layers in the flake, E_f is the exfoliation energy per carbon atom and m_C is the mass of a carbon atom, s is shear displacement of the graphite flake and l is the length of the flake. Recent experiments have shown the microscopic graphite flakes of thickness about 100 nm can reach 25 m/s, in quantitative agreement with the above formula[14]. For graphene, by extrapolating to $N = 1$, we deduce retraction speeds >400 m/s should be attainable.

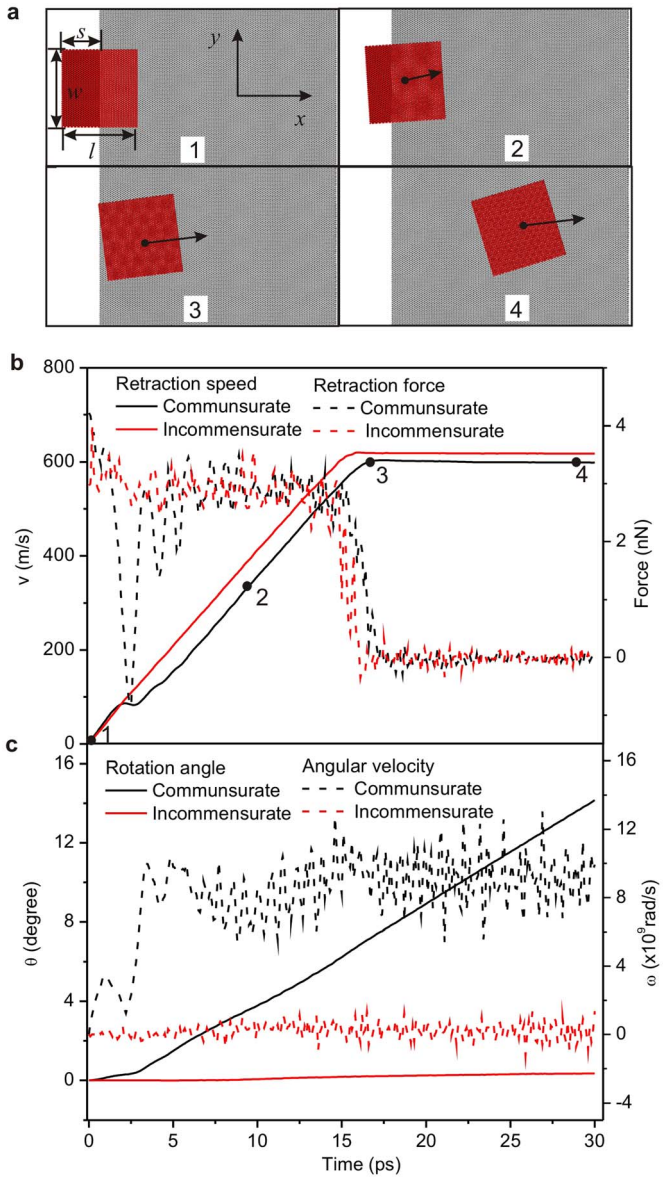

Figure 1 | Retraction motion of the graphene flake. Four snapshots (a) of the graphene flake of initial commensurate state during retraction where the direction and magnitude of the sliding speed are indicated by the arrows. The retraction speed and retraction force in x direction for initial commensurate and incommensurate state are recorded in (b). The four numbers are corresponding to the four snapshots in (a). (c) The rotation angle and angular velocity of the flake.

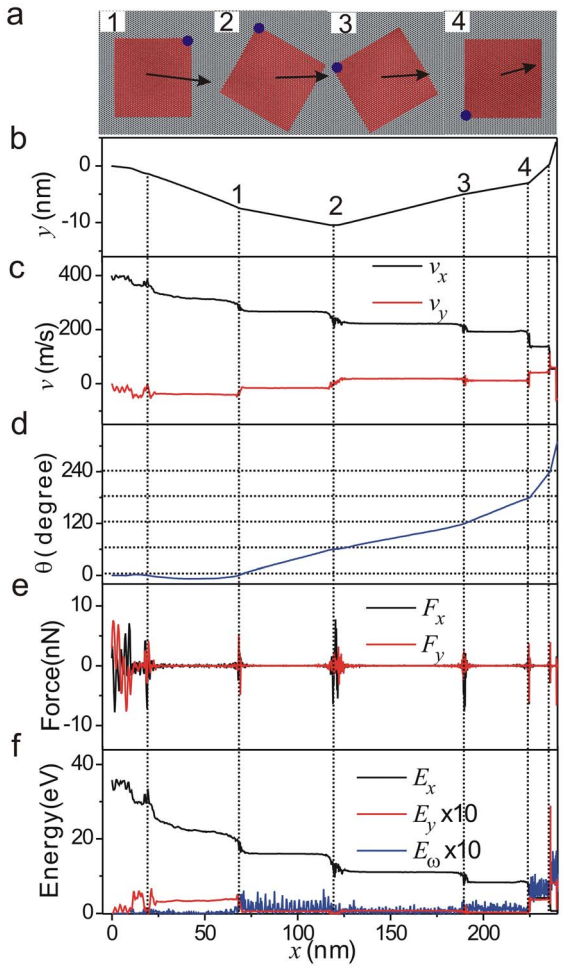

Figure 2 | Flake dynamics after launch at 400 m/s. Four snapshots (a) of the instantaneous orientation where the arrows indicate the direction and magnitude of the sliding speed and the frictional scattering at four points indicated on the flake trajectory (b). The speed components of the flake v_x and v_y (c), show stepwise changes at each scattering. The flake rotation θ (d) shows frictional scattering occurring primarily at high-symmetry angles (multiples of 60°). The force components acting on the flake, F_x and F_y (e) show large oscillatory variations at each scattering. The kinetic energy component E_x decays within about 1 ns to less than 10% of its initial value (f), and becomes comparable to E_y and E_ω.

To investigate the sliding behavior of a two-dimensional nanoscale graphene flake at such speeds, we employ molecular dynamics simulations using the Gromacs code[19] with Drieding force field to describe both the intra-layer and inter-layer interaction between carbon atoms of graphene[20]. The intra-layer interaction is consisted by bond stretching, bond-angle bending and dihedral angle torsion, while the inter-layer interaction is described by Lennard-Jones van der Waals potential. The parameters in the potential function are validated by correctly characterizing the structural and mechanical properties of different carbon nanostructures[21–23]. A graphite substrate is modeled by two layers of graphene in A–B stacking with the size of 30 nm × 20 nm where the bottom layer is fixed during the simulation. The moving graphene flake is modeled by one layer graphene with the size of 10 nm × 10 nm. Here two types of motion are studied in our simulations: the retraction motion and high speed sliding of the graphene flake, where the time step in all of our simulations is 1fs. For the retraction motion the top graphene flake is sheared away from the substrate with a half of its length $s = l/2$, as illustrated in Fig. 1a and free boundary conditions are applied to the substrate. For the simulation of the high speed sliding the graphene flake is placed on the center of the substrate and periodic boundary conditions are applied to the substrate. The whole system is first energy minimized by conjugate gradient method, and then the sliding speed is applied to the graphene flake. Here, the micro-canonical assemble is used in all of the simulations in coordination with the previous works of studying the frictional behavior of graphene[16,17].

The suspended graphene flake is released to simulate the retraction motion and the retraction speed, force, rotation angle and angular velocity of the graphene flake are recorded, as shown in Fig. 1b–c. Here, the retraction speed is the speed of the center of mass (COM) of the sliding flake; the rotation angle is defined as the angle rotated to its COM. The retraction force is calculated as the force between the substrate and the flake during retraction through the Lennard-Jones van der Waals potential defined before. Two types of initial conditions are considered: the first is the graphene flake commensurate

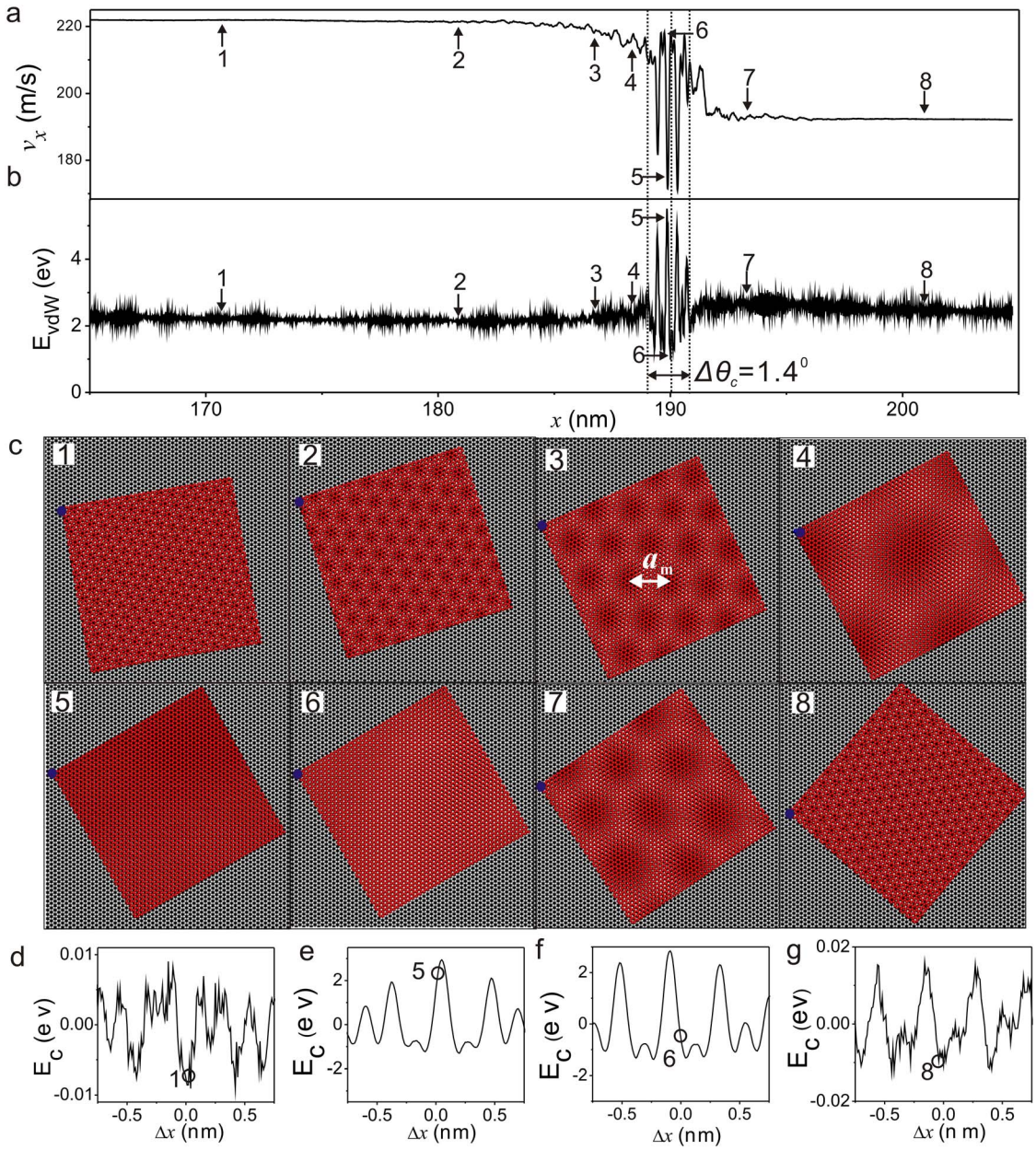

Figure 3 | Close-up of frictional scattering. Variation of the speed component v_x (a) and the van der Waals bonding energy E_{vdW} (b) as flake displacement along the x-direction, before, during and after a scattering event. Numbers indicate the snapshots of the flake (c). Vertical dotted lines in (a) and (b) indicate the angular width $\Delta\theta_c$ of the coherent region where $a_m > 2l$. The instantaneous corrugation potential, E_c, felt by the flake, for relative displacement in the x-direction about the flake's actual position (indicated by a circle) is shown before (d), during (e,f) and after (g) frictional scattering.

with the substrate; the second is the graphene flake incommensurate with the substrate where the orientation of the moving graphene flake is 90° misaligned to the substrate. Although the suspended graphene flake is very easy to fold and wrinkle at finite temperature, the length of the suspended graphene flake in our simulation is 5 nm which is hard to fold. Besides, the initial temperature of the whole system is 0 K and after releasing the graphene flake quickly retracts back, so the flat configuration is well kept. The maximum retracting speeds for the two cases are about 600 m/s which are consistent with the simple formula prediction. However, for the commensurate case the retraction is accompanied by the rotation at very beginning of the retracting which is corresponding to a large fluctuation of the retraction force, see the retraction force in Fig. 1b and angular velocity in Fig. 1c. After that the angular velocity is almost constant and the fluctuation of the retraction force quickly decreases. As the rotation the final retraction speed for the commensurate state is smaller than the incommensurate state.

Based on our results the commensurate state seems unstable for high sliding speed of the graphene flake and the graphene flake will automatically rotate to avoid the commensurate state. This is different from the previous works at low sliding speed where the commensurate state is the most stable state[11,12]. In what following we will simulate the high-speed sliding behavior of the graphene flake and find ways to reduce the sliding friction in such speed.

Results presented in Fig. 2 are for a 10×10 nm^2 flake launched at $v_{max} = 400$ m/s along the armchair direction of the substrate by adding the same velocity 400 m/s in x direction to every atom in the sliding flake. The sliding distance corresponding to 1 time step

(1fs) at v_{max} is less than 0.0004 nm. The initial state of the flake and substrate is an energy minimum state with A–B stacking alignment, and the initial temperature of the whole system is 0 K. The sliding speed, rotation angle, angular velocity and force are defined same as the ones in the retraction simulations. The sliding behavior in Figure 2b shows the trajectory of the flake, with sporadic changes in the direction of motion indicated by vertical dashed lines. For reasons that will become apparent shortly, we refer to these events as frictional scattering. Snapshots in Fig. 2a show each scattering event occurs when the flake is briefly crystallographically aligned with the substrate. At lower speed, this alignment would result in lock-in. But at high speed, the flake has sufficient kinetic energy to escape lock-in.

Figure 2c shows the component of the sliding speed along the x-direction, v_x, dropping in discrete steps at each scattering, with similar stepwise variations for v_y. The evolution of flake rotation angle, plotted in Fig. 2d, indicates that the flake angular velocity, ω, also changes abruptly at each scattering which is similar to the rotation in the retraction in Fig. 1c. Fig. 2e shows that scattering events subject the flake to large oscillatory forces in both x and y directions, producing abrupt changes of direction and velocity. In Fig. 2f, the linear kinetic energy components E_x and E_y in the x- and y-directions and the rotational kinetic energy E_ω of the flake are displayed. For better comparison we enlarge 10 times of E_y and E_ω in Fig. 2f. Since E_y and E_ω remain small throughout, we conclude that the initial kinetic energy of the flake is primarily dissipated into vibrational energy, with enhanced dissipation at each scattering. After ~1 ns, the sliding speed is smaller than 100 m/s, with E_x and E_y reaching similar magnitudes, and the flake moving randomly. Since the micro-canonical assemble is applied in the simulation, the whole system will be heated up as the dissipation of the translational speed of the sliding flake. However the substrate in our simulation (30 × 20 nm) is much larger than the sliding flake (10 × 10 nm), we estimate the temperature raising after dissipating all of the translational kinetic of the sliding flake is smaller 10 K.

To study the effect more closely, we zoom in on a region of frictional scattering in Fig. 3. The flake speed component, v_x, and van der Waals bonding energy between flake and substrate, E_{vdW} which is the van der Waals energy between the flake and substrate during the sliding, are displayed in Figs. 3a–b, respectively, and show rapid oscillations near alignment. Fig. 3c shows eight snapshots of the moiré pattern generated by the overlap of flake and substrate lattices, at different points indicated in Figs. 3a–b. When the flake is rotationally misaligned with the substrate, the moiré pattern has a small unit cell size, a_m. This means the spatial phase of flake atoms relative to the substrate potential oscillates rapidly across the flake. The result is a very small net corrugation potential for the flake as a whole: this is the origin of superlubricity for incommensurate lattices.

As the flake rotates into alignment, a_m expands (snapshots 1–4). Near alignment, once $a_m \gg l$, where l is the linear size of the flake, all flake atoms are nearly in phase with the substrate (snapshots 5, 6) and the net corrugation potential experienced by the flake increases abruptly, resulting in scattering. The corrugation potential drops again once the flake rotates sufficiently far out of alignment (snapshots 7, 8). Here the corrugation potential E_c is defined as the van der Waals energy between the flake and substrate by displacing the flake relative to flake's actual position along its instantaneous sliding speed, and recalculating E_{vdW} keeping all other parameters fixed. The variation of the corrugation potential, E_c, before, during and after alignment is shown in Figs. 3d–g. Near alignment (snapshots 5, 6) E_c is ~100x larger than during superlubricity, and the flake is subject to large potential gradients as indicated in Figs. 3e, f.

In the reference frame of the moving flake, the fundamental Fourier component of the substrate potential along the x-direction appears as a travelling wave of wavelength $\lambda = d$, where d is the in-plane lattice constant of graphite. When rows of atoms in the flake align with crests of this wave, there is a maximum oscillatory force acting on the flake. This corresponds to the condition for Bragg scattering $2d\sin\theta = n\lambda$, at normal incidence with $n = 2$. (For odd n, the force on neighbour rows cancels out.)

Since frictional scattering depends on the crystallinity of the flake, it will not be observed for diffusion of single atoms or small molecules at similar velocities[24]. Also, since frictional scattering depends on rotation in a plane, it is an intrinsically two-dimensional effect, physically distinct from velocity-dependent resonances observed in one-dimensional models[11] and nanotube simulations[21].

We can derive the angular width $\Delta\theta_c$ of the coherent region where $a_m \gg l$ using the standard moiré fringe formula[25] $a_m = d/(2|\sin(\Delta\theta/2)|)$, where $\Delta\theta$ is the rotation angle relative to alignment. Substituting for $a_m = 2l$ as a lower bound for coherence across the flake gives $\Delta\theta = d/2l$ in the small angle limit. Since $\Delta\theta$ is symmetric around the aligned position, $\Delta\theta_c = d/l$. This is identical to the Scherrer equation for a crystallite of dimension l and radiation of wavelength $\lambda = d$, for the case of normal incidence, emphasizing the mathematical analogy with Bragg scattering, which has been employed in the previous works to describe the interlocking between two contact surfaces[26,27]. Substituting $d = 0.246$ nm, the lattice constant of graphite and $l = 10$ nm gives $\Delta\theta_c = 1.4^\circ$. This angular width is plotted in Fig. 3b, and agrees with the range where E_{vdW} oscillates rapidly.

How robust an effect is frictional scattering? We have studied it as a function of several parameters, such as size of the graphene flake, temperature of the system and initial orientation of the graphene

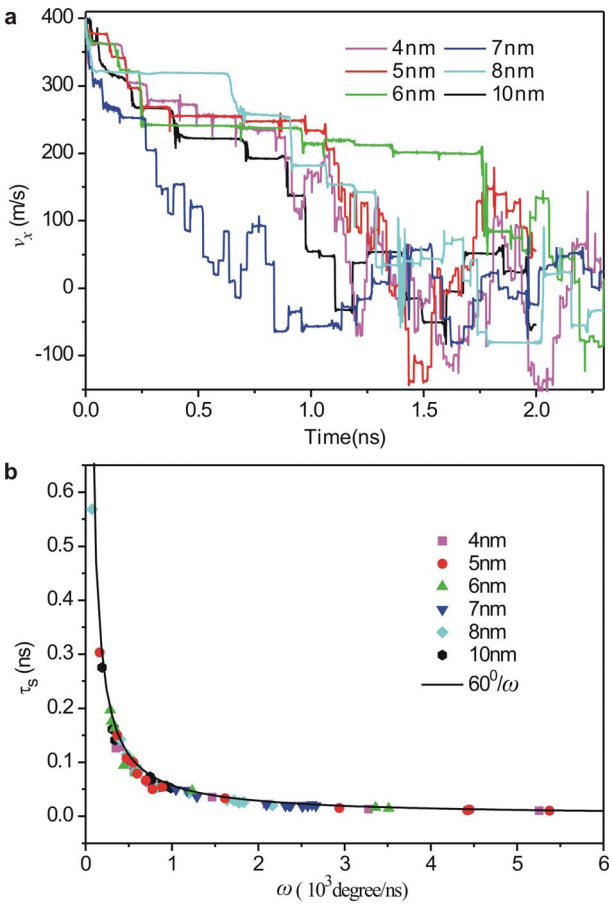

Figure 4 | The influence of flake size. Comparison of decay of the speed component v_x versus time after launch for different flake sizes (a) shows similar behavior for all sizes. (b) The duration of intervals of superlubricity, τ_s, depends inversely on the average angular velocity of the flakes during the intervals.

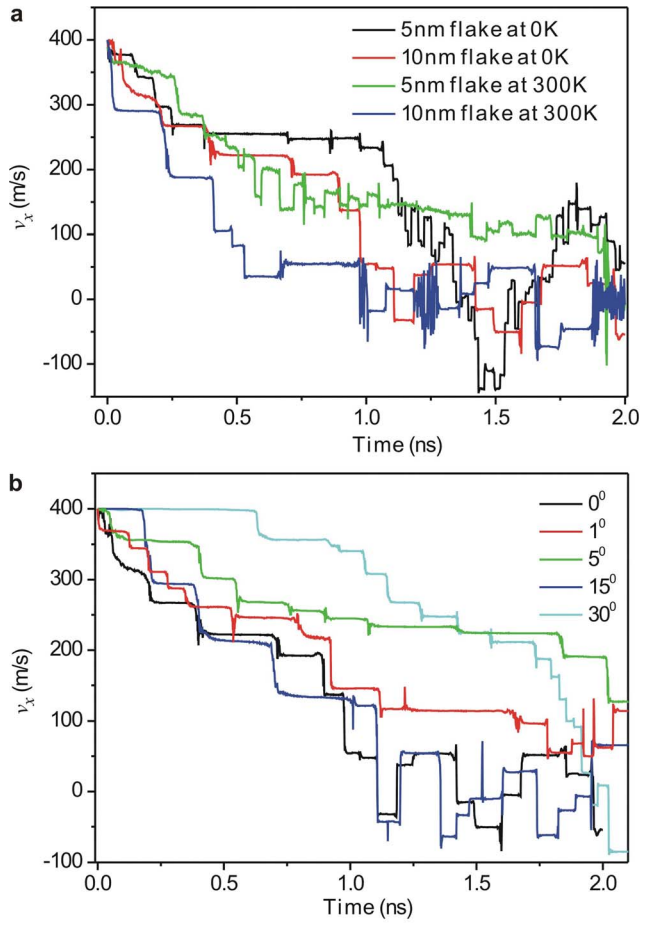

Figure 5 | The sliding behavior for different initial conditions. (a) The sliding behavior of 5×5 nm^2 and 10×10 nm^2 flakes launched initially at 0 K and 300 K. (b) The sliding behavior of 10×10 nm^2 flake for different orientation (the misalignment between the flake and the substrate is from 0° to 30°).

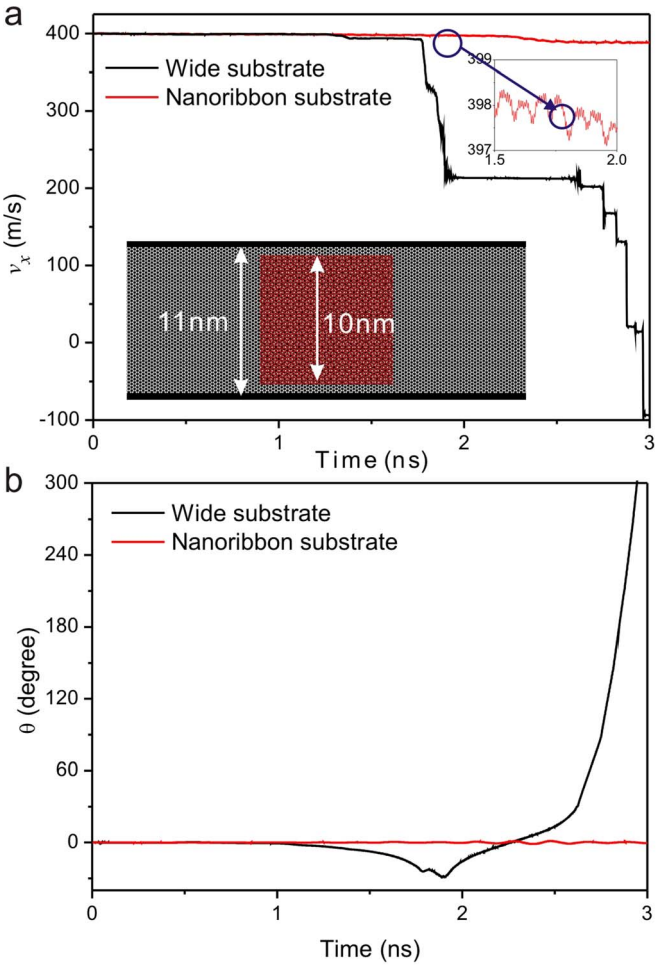

Figure 6 | The nanoribbon substrate. (a) The comparison of speed component v_x versus time for nanoribbon substrate and wide substrate. The lower inset is configuration of nanoribbon substrate. The upper inset shows a small oscillation of the forward speed. (b) The rotation angle of the graphene flake for nanoribbon substrate and wide substrate.

flake. For example, we find that for flakes with sizes from 4×4 nm^2 to 10×10 nm^2, the overall behavior is similar; the forward sliding for all flakes being dissipated within 2 ns, see Fig. 4a. The sliding speed in x direction sometimes increases when it is smaller than 100 m/s which is consistent with the previous work[16]. However as the sliding flake in our simulation is much larger than the nanoparticle (~250 Au atoms) studied in the previous work[16], the Brownian motion can't activate the sliding flake overcoming the energy barrier of the commensurate state. As shown in Fig. 2, the kinetic energy in y direction and rotation reaches the same level when the sliding speed in x direction is smaller than 100 m/s. Therefore, the kinetic energy transfer among the three modes may cause the increasing of the sliding speed in x direction.

Here, the intervals of superlubricity, τ_s, vary widely. Detailed analysis, summarized in Fig. 4b, shows that τ_s depends primarily on the flake angular velocity, ω, according to a simple relationship $\tau_s = 60°/\omega$. In other words, the rate of frictional scattering is simply determined by the rate of crystallographic alignments. Roughly, τ_s increases as the size of the sliding graphene flake increases. This is because the rotational inertia increases with the size of the graphene flake and for larger size flake the angular velocity is smaller. However the changes of the sliding speed are very complicated and highly dependent on the instantaneous state of the sliding flake which will be systematically studied in our future works.

The sensitivity of the results to initial temperature and flake orientation are given in Fig. 5. The simulated system is first equilibrated at the given temperature for 50ps by Nose-Hoover thermostat. Then the initial sliding speed of 400 m/s is added to the sliding flake and the thermostat is removed in the simulation afterward. The result for 5×5nm^2 and 10×10 nm^2 flakes launched initially at 0 K and 300 K show similar qualitative behavior, with regions of superlubricity punctuated by frictional scattering, see Fig. 5a. Detailed inspection shows a higher degree of noise for the high-temperature simulations, which is consistent with expectations for the impact of temperature. Simulations at T = 0 K, but for different initial orientations of the flake when it is launched, show overall similar qualitative behavior, with the sliding speed of all flakes decaying within 2ns, see Fig. 5b. For the initial misalignment between the sliding flake and the substrate (such as the rotation 30° in Fig. 5b) the initial superlubricity state can last a longer time. However after the first frictional scattering it becomes the similar frictional scattering behavior as the initial alignment case. We have also tested other flake shapes and varied substrate boundary conditions. In all cases we observe a similar stepwise decay, indicating that this is a computationally robust effect.

Based on the above analysis, we conclude that frictional scattering is the main source of sliding friction of the graphene nanoflakes on graphite in the ballistic friction regime. Based on this insight, we now explore two routes to suppressing frictional scattering in order to achieve persistent superlubricity at high speed.

Firstly, we introduce a graphene nanoribbon as a substrate to constrain the rotational motion of the graphene flake during sliding.

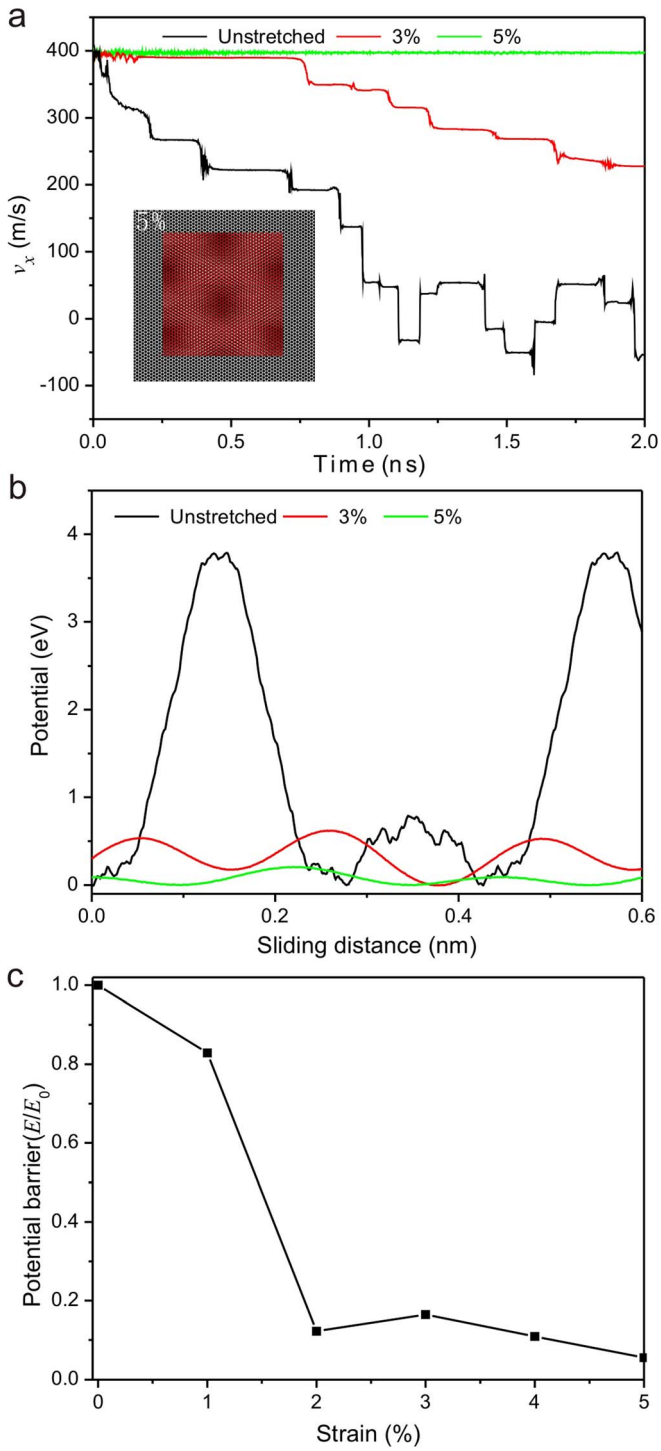

Figure 7 | The stretching substrate. (a) The comparison of speed component v_x versus time for stretched substrate and unstretched substrate. The lower inset is the configuration of 5% stretched substrate. (b) The sliding potential for different stretched substrate. (c) The relation between the sliding energy barrier and stretched strain.

Such graphene nanoribbons can be generated by the lithographic patterning[28] or chemical methods[29] with desired shapes and dimensions. In Fig. 6a, we launch a 10 × 10 nm^2 flake on a graphitic nanoribbon of width 11 nm, with the flake rotated 90° relative to the normal AB stacking of the nanoribbon. The sliding speed of the flake decays by less than 3% with the temperature increasing less than 1 K in the simulation time of 3 ns, compared with complete decay of the forward motion for the unconstrained flake. The nanoribbon acts as a frictional waveguide, periodically reflecting the flake off its edges, producing small velocity oscillations shown in the upper inset of Fig. 6a, and limiting flake rotation to ±1°, see Fig. 6b. However, for wide substrate as it can't constrain the rotation of the flake, the fictional scattering occurs when the flake first rotates 30° to encounter the commensurate state, see Fig. 6b. Therefore the sliding velocity rapidly decreases as the results in Fig. 5b. The waveguide has a speed cutoff: smooth sliding ceases below ~15 m/s, a typical velocity for transition to stick-slip motion in atomic-scale simulations[30].

In a similar manner, we can achieve suppression of friction by biaxial stretching of the substrate. Such stretching of a graphitic surface can be achieved by uniformly stretching a PDMS film with graphene attached on it[31]. For example, Kim et al.[31] have found the graphene can sustain as much as 30% uniaxial tensile strain without failure. Besides, as the lattice mismatch between the substrate and the graphene there is some residual strain in the epitaxial grown grahene which may be another routine to generate stretching in the graphene substrate[32]. Because of the very weak interlayer van der Waals interaction, the deformation of the substrate can not transfer to a flake adsorbed. So in this way we can envisage generating an initial lattice-constant mismatch between the substrate and the flake, as indicated by the moiré patterns in the inset of Fig. 7a. We have modeled the sliding behavior of a 10 × 10 nm^2 flake on a strained graphite substrate, with strains of 3% and 5%. For the 3% extension, the flake still undergoes scattering events, but with a reduced impact on the forward speed. For the 5% tension, there is no evidence of scattering events over the time of the simulation, 2ns. This is consistent with the notion that the flake can no longer be in exact commensuration with the substrate, due to its significantly different lattice parameter. The sliding potential E_{vdW} for different stretched substrates is given in Fig. 7b. Here the orientation of the flake is same as the substrate and the sliding direction is in armchair direction same as the direction of the initial launched speed. By applying strain to the substrate the sliding potential barrier of the graphene flake is significantly reduced. As in Fig. 7c the sliding energy barrier for the 5% stretched substrate is only 5% of the value of unstretched substrate. This is the origin of low sliding resistance for stretched substrate.

In conclusion, the motion of a nanoscale graphene flake on graphite at high speed is dominated by frictional scattering, where large oscillatory forces act each time the flake rotates through crystallographic alignment with the substrate. Frictional scattering is intrinsically two dimensional, and can be suppressed by constraining the flake to move along a quasi-one-dimensional frictional waveguide or stretching the substrate to generate lattice mismatch. In addition, we have introduced a simple shearing mechanism as a practical way to accelerate nanoscale flakes of graphene to velocities >100 m/s where ballistic friction occurs. These results should stimulate further experimental and theoretical interest in achieving persistent superlubricity on the nanoscale, a regime of considerable practical importance for future nanomechanical devices.

1. Urbakh, M., Klafter, J., Gourdon, D. & Israelachvili, J. The nonlinear nature of friction. *Nature* **430**, 525–528 (2004).
2. Luan, B. & Robbins, M. O. The breakdown of continuum models for mechanical contacts. *Nature* **435**, 929–932 (2005).
3. Mo, Y., Turner, K. T. & Szlufarska, I. Friction laws at the nanoscale. *Nature* **457**, 1116–1119 (2009).
4. Socoliuc, A. *et al.* Atomic-scale control of friction by actuation of nanometer-sized contacts. *Science* **313**, 207–210 (2006).
5. Lantz, M. A., Wiesmann, D. & Gotsmann, B. Dynamic superlubricity and the elimination of wear on the nanoscale. *Nature Nanotech.* **4**, 586–591 (2009).
6. Hirano, M. [Superlubricity of Clean Surfaces] *Superlubricity* [A. Erdemir & J. M. Martin(eds.)] (Elsevier, Amsterdam, 2007).
7. Shinjo, K. & Hirano, M. Dynamics of Friction - Superlubric State. *Surf. Sci.* **283**, 473–478 (1993).
8. Hirano, M., Shinjo, K., Kaneko, R. & Murata, Y. Observation of superlubricity by scanning tunneling microscopy. *Phys. Rev. Lett.* **78**, 1448–1451 (1997).
9. Dienwiebel, M. *et al.* Superlubricity of graphite. *Phys. Rev. Lett.* **92**, 126101 (2004).

10. Depondt, P., Ghazali, A. & Lévy, J. Self-locking of a modulated single overlayer in a nanotribology simulation. *Surf. Sci.* **419**, 29–37 (1998).
11. Filippov, A. E., Dienwiebel, M., Frenken, J. W. M., Klafter, J. & Urbakh, M. Torque and twist against superlubricity. *Phys. Rev. Lett.* **100**, 046102 (2008).
12. de Wijn, A. S., Fusco, C. & Fasolino, A. Stability of superlubric sliding on graphite. *Phys. Rev. E* **81**, 046105 (2010).
13. de Wijn, A. S., Fasolino, A., Filippov, A. & Urbakh, M. Low friction and rotational dynamics of crystalline flakes in solid lubrication. *Europhys. Lett.* **95**, 66002 (2011).
14. Yang, J. *et al.* Observation of high-speed microscale superlubricity in graphite. *Phys. Rev. Lett.* **110**, 255504 (2013).
15. Liu, Z. *et al.* Observation of microscale superlubricity in graphite. *Phys. Rev. Lett.* **108**, 205503 (2012).
16. Guerra, R., Tartaglino, U., Vanossi, A. & Tosatti, E. Ballistic nanofriction. *Nature Mater.* **9**, 634–637 (2010).
17. Lebedeva, I. V. *et al.* Fast diffusion of a graphene flake on a graphene layer. *Phys. Rev. B* **82**, 155460 (2010).
18. Zheng, Q. S. *et al.* Self-retracting motion of graphite microflakes. *Phys. Rev. Lett.* **100**, 067205 (2008).
19. Lindahl, E., Hess, B. & van der Spoel, D. GROMACS 3.0: a package for molecular simulation and trajectory analysis. *J. Mol. Model.* **7**, 306–317 (2001).
20. Mayo, S. L., Olafson, B. D. & Goddard, W. A. DREIDING: a generic force field for molecular simulations. *J. Phys. Chem.* **94**, 8897–8909 (1990).
21. Xu, Z. P. *et al.* Trans-phonon effects in ultra-fast nanodevices. *Nanotechnology* **19**, 255705 (2008).
22. Guo, Y. J., Karasawa, N. & Goddard, W. A. Prediction of Fullerene Packing in C60 and C70 Crystals. *Nature* **351**, 464–467 (1991).
23. Rivera, J. L., McCabe, C. & Cummings, P. T. Oscillatory behavior of double-walled nanotubes under extension: a simple nanoscale damped spring. *Nano Lett.* **3**, 1001–1005 (2003).
24. Hedgeland, H. *et al.* Measurement of single-molecule frictional dissipation in a prototypical nanoscale system. *Nature Phys.* **5**, 561–564 (2009).
25. Woan, G. *The Cambridge handbook of physics formulas.* (Cambridge University Press, Cambridge, 2000).
26. Müser, M. H. Structural lubricity: Role of dimension and symmetry. *Europhys. Lett.* **66**, 97 (2004).
27. Müser, M. H., Wenning, L. & Robbins, M. O. Simple microscopic theory of Amontons's laws for static friction. *Phys. Rev. Lett.* **86**, 1295 (2001).
28. Tapaszto, L., Dobrik, G., Lambin, P. & Biro, L. P. Tailoring the atomic structure of graphene nanoribbons by scanning tunnelling microscope lithography. *Nature Nanotech.* **3**, 397–401 (2008).
29. Li, X., Wang, X., Zhang, L., Lee, S. & Dai, H. Chemically derived, ultrasmooth graphene nanoribbon semiconductors. *Science* **319**, 1229–1232 (2008).
30. Braun, O., Peyrard, M., Bortolani, V., Franchini, A. & Vanossi, A. Transition from smooth sliding to stick-slip motion in a single frictional contact. *Phys. Rev. E* **72**, 056116 (2005).
31. Kim, K. S. *et al.* Large-scale pattern growth of graphene films for stretchable transparent electrodes. *Nature* **457**, 706–710 (2009).
32. Pan, Y. *et al.* Highly Ordered, Millimeter-Scale, Continuous, Single-Crystalline Graphene Monolayer Formed on Ru (0001). *Adv. Mater.* **21**, 2777–2780 (2009).

Acknowledgments

Y.L. acknowledges the support by the National Natural Science Foundation of China through Grants No. 11302163 and No. 11321062. Q.S.Z. acknowledges the financial support from National Natural Science Foundation of China through Grants No. 10832005, the National Basic Research Program of China through Grant No. 2013CB934200 and No. 2007CB936803.

Author contributions

Y.L. conducted all of the MD simulations and prepared the figures. F.G. developed the frictional scattering model used to explain the results and wrote the main manuscript text. Q.S. supervised the study and wrote the manuscript. All authors reviewed the manuscript.

Additional information

Competing financial interests: The authors declare no competing financial interests.

How to cite this article: Liu, Y.L., Grey, F. & Zheng, Q.S. The high-speed sliding friction of graphene and novel routes to persistent superlubricity. *Sci. Rep.* **4**, 4875; DOI:10.1038/srep04875 (2014).